Surveying GNSS Carrier Offset Modulations: Investigating Gabor Uncertainty Principle for Precise Time Delay and Frequency Offsets Estimation

Surveying GNSS Carrier Offset Modulations: Investigating Gabor Uncertainty Principle for Precise Time Delay and Frequency Offsets Estimation

Luca Morichi, Alex Minetto, Andrea Nardin, Fabio Dovis, *Politecnico di Torino, Turin, Italy*

BIOGRAPHY

Luca Morichi received a B.Sc. in Telecommunication Engineering in 2022 and a M.Sc. in Communication and Computer Networks Engineering in 2023, both from Politecnico di Torino (Turin, Italy). He is currently a Ph.D. student within the Navigation Signal Analysis and Simulation (NavSAS) group at Politecnico di Torino. His research is focused on the design and optimization of radionavigation signals and modulations for modernized MEO and LEO PNT services.

Alex Minetto received the B.Sc., and M.sc. degrees in Telecommunications Engineering from Politecnico di Torino, Turin, Italy and his Ph.D. degree in Electrical, Electronics and Communications Engineering, in 2020. He joined the Department of Electronics and Telecommunications of Politecnico di Torino in 2021 as researcher and assistant professor. His current research interests cover navigation signal design and processing, advanced Bayesian estimation applied to Positioning and Navigation Technologies (PNT) and applied Global Navigation Satellite System (GNSS) to space weather and space PNT.

Andrea Nardin received the M.Sc. degree in Telecommunications engineering and the Ph.D. degree in Electrical, Electronics and Communications Engineering, in 2018 and 2023, respectively, both from Politecnico di Torino, where he is currently a postdoctoral researcher. From 2018, he has been working on satellite navigation technologies with the Navigation Signal Analysis and Simulation (NavSAS) group at Politecnico di Torino and in 2021 he was a Visiting Doctoral Researcher at Northeastern University, Boston, MA, USA with the Information Processing Lab (IPL).

Fabio Dovis received his M.Sc. degree in 1996 and his Ph.D. degree in 2000, both from Politecnico di Torino, Turin, Italy. He joined the Department of Electronics and Telecommunications of Politecnico di Torino as an assistant professor in 2004 and as associate professor in 2014. Since 2021 he is a full professor. He coordinates the Navigation Signal Analysis and Simulation (NavSAS) research group. His research interests cover the design of GPS and Galileo receivers, advanced signal processing for interference and multipath detection and mitigation, as well as ionospheric monitoring.

ABSTRACT

In the last decades, the adoption of offset carrier modulations represented one of the main aspects in the modernization of Global Navigation Satellite System (GNSS) signals. Offset carrier modulations provide indeed specific signal characteristics and guarantee the desired performance trade-off in terms of bandwidth utilization and tracking jitter at the receiver. In light of this, ongoing signal design proposals for modernized GNSS, Low-Earth Orbit and navigation services cannot neglect fundamental findings in this direction. At the same time, the theoretical bounds governing time delay and frequency offset estimation have a direct impact on receivers state estimation when this task rely on the inference of signal-derived observables. In this context, the aim of this work is to investigate the inherent relationship between offset carrier modulation, i.e., spreading code chip shaping, and the bounds set by uncertainty principle about time delay and frequency offsets estimation of GNSS signals. The research addresses a surveying analysis of currently-adopted offset carrier modulations and the evaluation of their theoretical bounds associated to the respective analytical ambiguity functions. The study offers a methodology to synoptically compare different chip shaping and to characterize how this influences signals' time-frequency localization precision and estimation errors at the receiver, which has a direct impact on delay and frequency lock loops performance at the receiver tracking stage.

I. INTRODUCTION

In the domain of Global Navigation Satellite System (GNSS), the precise acquisition of code phase and frequency offset measurements is crucial. This process involves minimizing the peak region of the Cross-Ambiguity Function (CAF) across both time and frequency domains (Pratap and Per, 2010), which is essential for accurately determining pseudorange and Doppler observables. Sharper peaks in these domains correlate with enhanced precision, thereby improving state estimation performance.

The uncertainty principle, formalized in the late 1920s within the framework of quantum mechanics by Heisenberg, Kennard, Weyl, and Robertson, imposes fundamental limits on the precision with which pairs of conjugate variables, such as position and momentum, can be simultaneously determined (Heissenberg, 1930; Kennard, 1927; Robertson, 1929). According to Gabor theory, this has significant implications for signal processing, particularly in the simultaneous analysis of time and frequency signals. This principle highlights the inherent trade-off between time and frequency resolutions in radar and radionavigation theory, impacting the joint estimation of signal time delay and frequency offset relative to a local signal replica. A more localized signal in the time domain will have a broader bandwidth, and vice versa, affecting the uncertainties in time delay and frequency offset estimation within GNSS receivers.

Various optimization algorithms have been investigated to design offset carrier modulation schemes that minimize time delay uncertainty (Zhang et al., 2011a,b), often neglecting the precision of frequency offset estimation. Despite the significance of these findings, the authors have overlooked important theoretical relationships, particularly the well-established Gabor time-frequency localization principle and the fundamental limits set by Gaussian pulses (Haddad et al., 1993).

Accurate frequency offset estimation is crucial for proper carrier wipe-off during the conventional tracking stage of GNSS and for inferring Doppler shifts to estimate receiver velocity. Despite several works provided practical evidence about the independence of pseuodorange and frequency offset observables (Zocca et al., 2022), an accurate velocity estimation is tightly related to position state estimate in Bayesian estimation approach such as Kalman and particle filters. Error contributions from poorly designed signals are hence significant in positioning, navigation, and timing applications.

This study focuses on analytical aspects to reveal fundamental bounds as early indicators of suitable signal design. We introduce a semi-analytic methodology to evaluate offset carrier modulation performance based on the time-frequency localization principle and its relationship to precise code time delay and frequency offset estimation. To generalize the use of comprehensive trade-off metrics, we disregard the periodicity of the signal and codes, treating fundamental offset carrier modulation shapes as waveforms of finite duration, akin to radar impulsive signal analysis.

The objective of this work is twofold: to provide an analytical methodology for evaluating chip shaping performance concerning the time-frequency localization principle and to survey current state-of-the-art modulations in modern GNSS systems, bounding their performance against ideal pulse shaping. Furthermore, we introduce the concept of the uncertainty product as a metric for signal design trade-offs, offering a holistic perspective on GNSS subcarrier performance characterization. This methodology enhances the understanding of subcarrier chip shaping's impact on radionavigation signals' performance and establishes a foundation for informed decision-making in signal design and system optimization, thereby advancing radionavigation technology.

It is important to note that a similar analysis is lacking in the current literature. The increasing demand for new systems, such as LEO PNT and Lunar PNT, as well as the modernization of existing GNSS constellations, necessitates a detailed understanding of the most significant trade-off metrics. The authors are well-aware that signal design trade-offs must also contemplate for correlation ambiguity, resilience to interference and multipath, and several other key performance parameters (Yao and Lu, 2021; Hegarty, 2012). However, this work mostly address signal related aspects, with the discussion of receiver-side considerations deferred to complementary, future research.

The reminder of this paper is as follows. Section II revisit and formalize key theoretical concepts from signal theory, with a particular focus on time-frequency signal localization. Section III presents the simulation environment utilized for the synoptical analysis of the various offset carrier modulation. Section IV collects fundamental limits for state-of-the-art offset carrier modulation schemes and generalizes these results for extended trade-offs. Section V summarizes the main conclusions of the study.

II. BACKGROUND

1. Uncertainty principle in signal theory

The uncertainty principle in signal theory is tightly related to its counterpart in quantum mechanics. It is often referred to as the Gabor uncertainty principle, named after Dennis Gabor's 1946 article on the subject (Gabor, 1946). Gabor's uncertainty principle states that a signal cannot be localized simultaneously in the time and frequency domains with arbitrary precision. If the signal support is constrained in one domain, it must be broadened in the other. This highlights a fundamental trade-off between time and frequency resolution in signal processing.

The time-frequency localization of a signal pertains to its distribution across these respective domains. Mathematically, this relationship can be characterized by the variance, which quantifies the dispersion of a probability density function (pdf) around its mean.

Consider a generic signal in the time domain $s(t) \in L_2(\mathbb{R})$. The signal $s(t)$ is a square-integrable function over the real

numbers. Let $S(\omega)$ be its Fourier transform, which also belongs to $L_2(\mathbb{R})$. We define

$$p_s(t) = \frac{|s(t)|^2}{\int_{-\infty}^{+\infty} |s(t)|^2 dt} = \frac{|s(t)|^2}{E_s} \tag{1}$$

where E_s is the energy of the signal $s(t)$. The function $p_s(t)$ can be interpreted as a pdf over time, describing the distribution of the signal's energy in this domain. A dual formulation holds in the frequency domain. We can define

$$p_S(\omega) = \frac{|S(\omega)|^2}{\int_{-\infty}^{+\infty} |S(\omega)|^2 d\omega} = \frac{|S(\omega)|^2}{E_\omega} \tag{2}$$

where, E_ω represents the energy of the signal in the angular frequency domain. The function $p_S(\omega)$ is the distribution of the signal's energy across angular frequency. Relying on (1) and (2) it is possible to define the second-order central moment, i.e., the variance of the signal in the respective domains, as

$$\sigma_t^2 = \int_{-\infty}^{+\infty} (t - t_0)^2 \, p_s(t) \, dt = \frac{1}{E_s} \int_{-\infty}^{+\infty} (t - t_0)^2 \, |s(t)|^2 \, dt \tag{3}$$

$$\sigma_\omega^2 = \int_{-\infty}^{+\infty} (\omega - \omega_0)^2 \, p_S(\omega) \, d\omega = \frac{1}{E_\omega} \int_{-\infty}^{+\infty} (\omega - \omega_0)^2 \, |S(\omega)|^2 \, d\omega \tag{4}$$

where t_0 and ω_0 identify the mean in time and angular frequency domain respectively and can be written as shown below.

$$t_0 = \int_{-\infty}^{+\infty} t \, p_s(t) dt = \frac{1}{E_s} \int_{-\infty}^{+\infty} t |s(t)|^2 \, dt \tag{5}$$

$$\omega_0 = \int_{-\infty}^{+\infty} \omega \, p_S(\omega) \, d\omega = \frac{1}{E_\omega} \int_{-\infty}^{+\infty} \omega^2 |S(\omega)|^2 \, d\omega \tag{6}$$

In signal and radar theory (Levanon, 1988), the square roots of (3) and (4) are referred to as the root-mean-squared (RMS) duration and RMS bandwidth, respectively, with the latter also known as the Gabor bandwidth. These quantities determine the concentration of signal energy around its mean, serving as indicators of how localized the signal is in either the time or frequency domain.

An alternative formulation for (3) and (4) that is popular in literature (McDonough and Whalen, 1995) is as

$$\sigma_t^2 = \frac{1}{E_s} \int_{-\infty}^{+\infty} t^2 |s(t)|^2 \, dt - \left[\frac{1}{E_s} \int_{-\infty}^{+\infty} t |s(t)|^2 \, dt \right]^2 \tag{7}$$

$$\sigma_\omega^2 = \frac{1}{E_\omega} \int_{-\infty}^{+\infty} \omega^2 |S(\omega)|^2 \, d\omega - \left[\frac{1}{E_\omega} \int_{-\infty}^{+\infty} \omega |S(\omega)|^2 \, d\omega \right]^2 \tag{8}$$

This approach intuitively aligns the aforementioned definitions with the statistical definition of variance. It highlights that these quantities can be quantified as the expected value of the random variables squared minus the square of their expected value (Ross, 2010).

For the sake of completeness, Appendix VI.1 shows the equality between (3) and (7) and (4) and (8), respectively.

As demonstrated in the literature, tailoring signals for enhanced performance in either the time or frequency domain is a common practice in signal design (Zhang et al., 2011a,b). Specifically, it is feasible to design a signal with a small σ_t or σ_ω. However, when both domains are considered equally relevant, the limitations imposed by the uncertainty principle must be taken into account. In this case, instead of considering (3) and (4) separately, one can consider the *time-bandwidth product*, which is defined as the product of the two.

$$\sigma_t^2 \, \sigma_\omega^2 = \frac{\int_{-\infty}^{+\infty} (t - t_0)^2 \, |s(t)|^2 \, dt}{E_t} \frac{\int_{-\infty}^{+\infty} (\omega - \omega_0)^2 \, |S(\omega)|^2 \, d\omega}{E_\omega} \tag{9}$$

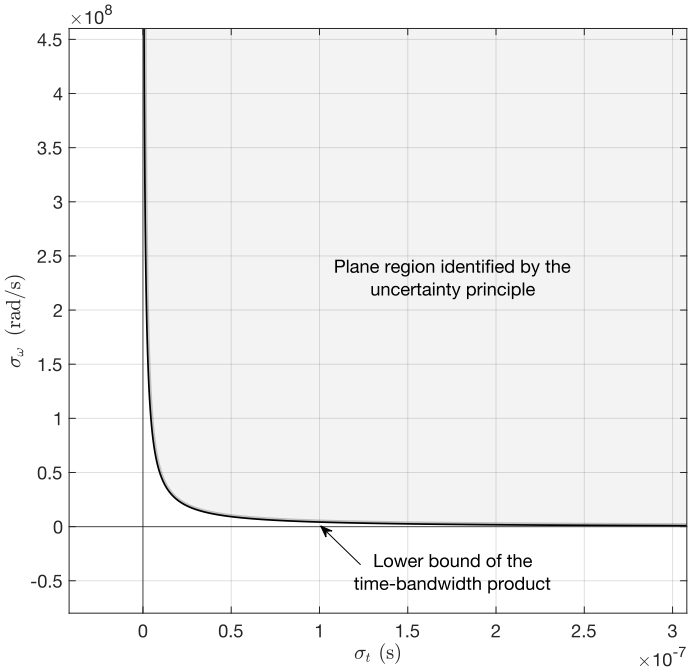

Figure 1: Time-bandwidth product hyperbola for the Gaussian pulse. Pulse observed over an interval $T_c = 9 \times 10^{-5}$ s, with the parameter α varying from 1×10^{-8} to 9.78×10^{-6}.

By assuming t_0 and ω_0 equal to 0 in (9) we can assume independence of the time-bandwidth product from time or frequency shift, respectively. As per Appendix VI.2, it can be shown that this assumption can be made without loss of generality because the time-bandwidth product is invariant to shifts in time or frequency. Its value solely depends on the signal's shape.

Furthermore, it can be proved (Boggess and Narcowich, 2015; Luise and Vitetta, 2009) that the product in (9) cannot be arbitrarily small; rather, a lower bound can be identified. Given the specific formulation of σ_t^2 and σ_ω^2, this lower bound has been formalized in (Papoulis, 1977), as

$$\sigma_t \sigma_\omega \geq \frac{1}{2} \tag{10}$$

where σ_t and σ_ω are the standard deviation in the two domain, obtained taking the square root of (3) and (4) respectively.

It is important to note that various formulations of this fundamental lower bound can be found in the literature, each presenting different constants in the second term. These discrepancies mainly arise from the different methods used to measure RMS bandwidth and RMS duration. For example, if the signal is characterized by a one-sided bandwidth and not expressed in angular frequencies, the constant becomes $\frac{1}{8\pi}$ instead of $\frac{1}{2}$ (Luise and Vitetta, 2009). Nonetheless, despite the differences in these constants, the underlying principle remains consistent. Additionally, it can be demonstrated that (10) holds with equality only if $s(t)$ is a Gaussian signal of the form $s(t) = Ae^{-(t/\alpha)^2}$ (Papoulis, 1977; Luise and Vitetta, 2009).

When equality holds, (10) describes a hyperbola in the first quadrant of a Cartesian plane, with the x-axis representing σ_t and the y-axis representing σ_ω. This hyperbola defines the performance in terms of the time-frequency localization of the Gaussian signal. For other signals, the points describing their time-frequency localization will lie within the region of the plane that is lower bounded by the hyperbola, as illustrated in Figure 1. Here, the hyperbola describes the points σ_t and σ_ω of a Gaussian signal observed over an interval $T_c = 9 \times 10^{-5}$ s, generated by varying the parameter α (ranging from 1×10^{-8} to 9.78×10^{-6}). The parameter α influences the width of the Gaussian bell in the time domain and inversely affects the dispersion of the signal energy in the frequency domain.

2. Performance Limits in time delay and frequency offset estimation

While the uncertainty principle presented in Section II.1 provides a natural theoretical lower bound on the localization of a signal in the time and frequency domains, the Cramér-Rao Lower Bound (CRLB) provides a practical lower bound on the variance of unbiased estimators.

Let us consider the estimation of the unknown time delay θ from a noisy signal observation

$$x(t) = s(t-\theta) + n(t) \tag{11}$$

where $s(t-\theta)$ is the delayed version of the transmitted signal $s(t)$ and $n(t)$ is a zero-mean additive white Gaussian noise.

In the presence of a sufficiently high signal-to-noise ratio (SNR), the CRLB proposed in (McDonough and Whalen, 1995) defines a lower bound for the uncertainty on the time delay estimation

$$\sigma_{\Theta}^2 \geq \frac{1}{2\,\mathrm{SNR}\,\sigma_{\omega}^2}. \tag{12}$$

where σ_{ω}^2 is the square of the RMS bandwidth defined in (4). It is important to highlight the inversely proportional relationship between the CRLB and the square of the RMS bandwidth. This means that a greater RMS bandwidth, indicating a signal that is less localized around its mean in the frequency domain, reduces the lower bound on the variance of the time delay estimator, allowing for more precise estimates. This aligns with the fact that increasing the RMS bandwidth results in the signal being more localized in time. For radionavigation signals, this translates to higher ranging accuracy.

For what concerns the estimation of frequency offset ω_o, let us consider a noisy observation

$$x(t) = s(t)e^{(j\omega_o t)} + n(t) \tag{13}$$

where $s(t)\,e^{(j\omega_o t)}$ is the version of the transmitted signal affected by the frequency offset and $n(t)$ is a zero mean additive white Gaussian noise. Following the derivation found in (McDonough and Whalen, 1995), under the assumption of having a sufficiently high SNR we obtain that the variance on the frequency offset estimate is lower bounded by:

$$\sigma_{\Omega}^2 \geq \frac{1}{2\,\mathrm{SNR}\,\sigma_{t}^2}. \tag{14}$$

From (14) it is possible to see the dual form with respect to (12). In this case in the denominator is the square of the RMS duration expressed as in (3). In this case, it can be observed that the estimation performance improves as the frequency localization of the signal improves.

Moreover, it is worth noting that in the GNSS domain, it is possible to substitute the value of SNR for the value of Carrier-to-Noise-density ratio (C/N_0) in (12) and (14) without affecting the consistency of the formula (Angelo, 2010).

III. METODOLOGY

1. Simulation framework

In this study, we focused on the impact of chip shape on the fundamental limits presented in Section II. To investigate this impact, we adopted a semi-analytical method, applying the limit formulas to numerically generated signals. To achieve this, we considered an observation time equal to T_c centered at zero. Figure 2 illustrates the chip shapes of the various modulations examined. To ensure a fair analysis, we normalized each chip to have unit energy by dividing the signal over time by the square root of its own energy.

Our research focused on Binary Offset Carrierr (BOC) subcarrier modulations, which are widely used by various GNSS, and corresponding Sinusoidal Offset Carrier (SOC) modulations. The modulations under investigation are listed in Table 1.

a) BOC modulation

BOC is the most popular offset carrier modulation employed in the definition of GNSS subcarriers. It involves modulating a binary signal onto an offset carrier, creating a signal with two symmetrical frequency components relative to the central carrier. BOC is a binary modulation with two levels, $[+1, -1]$, derived from a sinusoidal waveform (Ávila Rodríguez, 2008).

This modulation is commonly referred to in the time domain as BOC(m,n), where m and n define the subcarrier frequency $f_{sc} = \mathrm{m} \times 1.023\,\mathrm{MHz}$, and the chip rate $R_c = \mathrm{n} \times 1.023\,\mathrm{MHz}$, respectively. A key parameter in this modulation is the number of subcarrier periods within a chip, given by $\xi = \frac{\mathrm{m}}{\mathrm{n}}$. More information on the BOC modulations analyzed is given in Table 1.

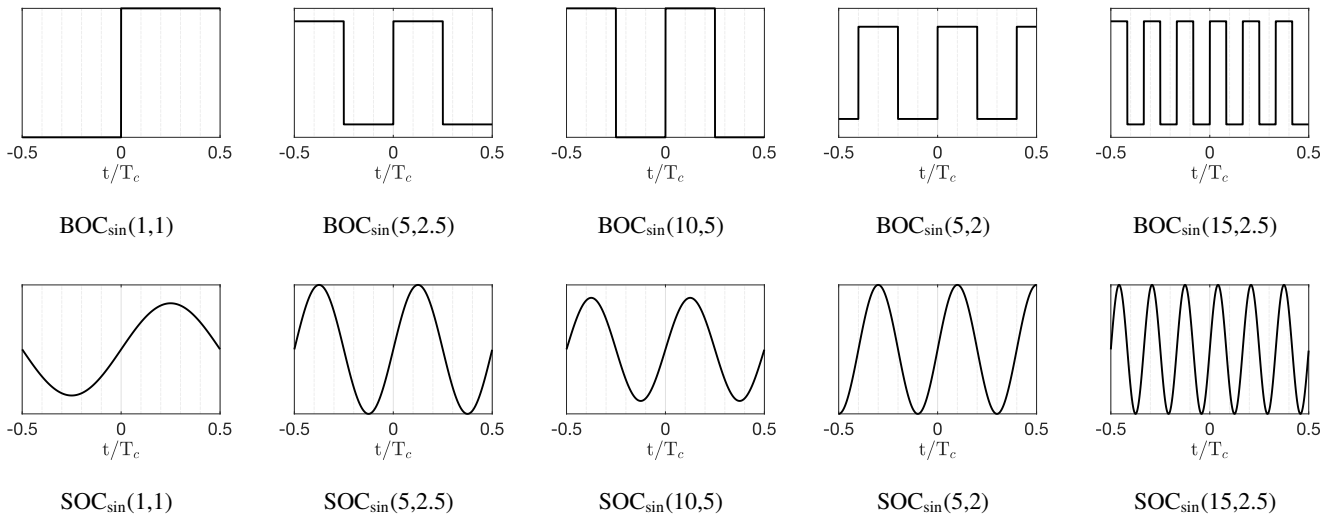

Figure 2: Offset carrier modulation under test definedin time domain over a support $\pm T_c/2$

b) SOC modulation

SOC modulation, like BOC, is used to modulate a binary signal and shift the spectrum. However, while BOC is a binary modulation derived from a sinusoidal waveform, SOC is not binary (Ávila Rodríguez, 2008). Similar to BOC, SOC modulation is described by two parameters, m and n. The value of m represents the subcarrier frequency f_{sc} in multiples of the base frequency 1.023 MHz, while the value of n represents the chip rate R_c in multiples of the base frequency 1.023 Mcps. Again, it is possible to identify the number of subperiods as $\xi = \frac{\mathrm{m}}{\mathrm{n}}$. More information on the SOC modulations analyzed is given in Table 1.

c) Gaussian Pulse

The Gaussian pulse was generated to serve as a benchmark for comparing the theoretical bounds we analyzed. It is defined as:

$$s(t) = e^{-(t/\alpha)^2} \tag{15}$$

where α is a parameter that influences the pulse width in the time domain. To have a comparable pulse with the other chips, a T_c consistent with the others is chosen. The parameter α can have an arbitrary value, but it is generally set to a fraction of T_c to ensure the pulse is mostly contained within T_c. We refer to the Gaussian pulse in the time domain as Gaussian(γ, n), where γ is the fraction of T_c we want to consider and n affects the duration of the chip, similar to the BOC and SOC cases.

d) Time and frequency axes

Defined T_c according to the chosen modulation, we set the time axis n_t as:

$$n_t = \left\{ t_n \mid t_n = -\frac{T_c}{2} + nT_s,\ n = 0, 1, 2, \ldots, N-1 \right\} \tag{16}$$

where T_s represents the sampling period, defined as the inverse of the sampling frequency F_s, which is set to $F_s = 40$ MHz in the simulation. N represents the number of samples and is defined as T_c/T_s.

As for the frequency domain, each $s(t)$ signal was transformed using the FFT function of MATLAB. The frequency axis was generated by calculating the frequency resolution $\Delta f = F_s/N$. This resulted in an axis ranging from $-\frac{F_s}{2}$ to $\frac{F_s}{2}$ with increments of Δf.

$$k_f = \left\{ f_k \mid f_k = -\frac{F_s}{2} + k \cdot \Delta f,\ k = 0, 1, 2, \ldots, N-1 \right\} \tag{17}$$

This frequency axis was then converted to the angular frequency axis $k_\omega = 2\pi k_f$.

Table 1: Selected BOC and SOC modulations.

Modulation (m, n)	f_{sc} (MHz)	R_c (Mcps)	ξ (m/n)
$\text{BOC}_{\text{sin}}(1,1)$ [1]	1.0230	1.023	1
$\text{SOC}_{\text{sin}}(1,1)$ [2]			
$\text{BOC}_{\text{sin}}(5,2.5)$ [1]	5.1150	2.5575	2
$\text{SOC}_{\text{sin}}(5,2.5)$ [2]			
$\text{BOC}_{\text{sin}}(10,5)$ [1]	10.2300	5.1150	2
$\text{SOC}_{\text{sin}}(10,5)$ [2]			
$\text{BOC}_{\text{sin}}(5,2)$ [1]	5.1150	2.0460	2.5
$\text{SOC}_{\text{sin}}(5,2)$ [2]			
$\text{BOC}_{\text{sin}}(15,2.5)$ [1]	15.3450	2.5575	6
$\text{SOC}_{\text{sin}}(15,2.5)$ [2]			

[1] BOC_{sin}: $s(t) = \text{sign}[\sin(2\pi f_{sc} t)]$
[2] SOC_{sin}: $s(t) = \sin(2\pi f_{sc} t)$

2. Calculation of theoretical limits

To evaluate theoretical bounds, we applied

$$\sigma_t^2 = \frac{1}{E_s} \int_{-\infty}^{+\infty} (t - t_0)^2 \, |s(t)|^2 \, dt \rightarrow \sigma_{n_t}^2 = \frac{1}{E_{s_n}} \sum (n_t - n_{t0})^2 \, |s(n_t)|^2 \, T_s \tag{18}$$

where

$$E_s = \int_{-\infty}^{+\infty} |s(t)|^2 dt \rightarrow E_{s_n} = \sum |s(n_t)|^2 \, T_s \tag{19}$$

$$t_0 = \frac{1}{E_s} \int_{-\infty}^{+\infty} t \, |s(t)|^2 dt \rightarrow n_{t0} = \frac{1}{E_{s_n}} \sum n_t \, |s(n_t)|^2 \, T_s \tag{20}$$

As for the frequency domain, a similar conversion was made. Where instead of T_s the summation is multiplied by $\Delta\omega = 2\,\pi\,\Delta f$, and instead of $s(n_t)$, $s(k_\omega)$ is used. The discrete formulations of the various limits were tested and validated using numerical methods for calculating integrals.

As for the analyses on CRLB, they depend on the values of C/N_0. For the analyses conducted, we selected a range of C/N_0 from 0 to 50 dB-Hz with a step of 5 dB-Hz.

$$C/N_{0_{\text{dB-Hz}}} = \left\{ C/N_{0_{\text{dB-Hz}_i}} \mid C/N_{0_{\text{dB-Hz}_i}} = 0 + i \cdot 5, \; i = 0, 1, 2, \ldots, 50 \right\} \tag{21}$$

IV. RESULTS

1. Analysis of the time-bandwidth product

Figure 3 illustrates the distribution of time-bandwidth product ($\sigma_t \times \sigma_\omega$) of the various modulation chip shapes analyzed with respect to uncertainty principle.

The black hyperbola represents the theoretical lower bound imposed by uncertainty principle, (10), achievable only by the Gaussian impulse. By adjusting the parameter α, the Gaussian impulse can be expanded or contracted in the time domain, encompassing all points along the solid hyperbola

Above the hyperbola, the highlighted area indicates where the time-bandwidth product exceed the lower bound, defining the region that satisfies uncertainty principle. Each point placed in this area corresponds to a pair of values $(\sigma_t, \sigma_\omega)$ associated with a specific modulation chip shape.

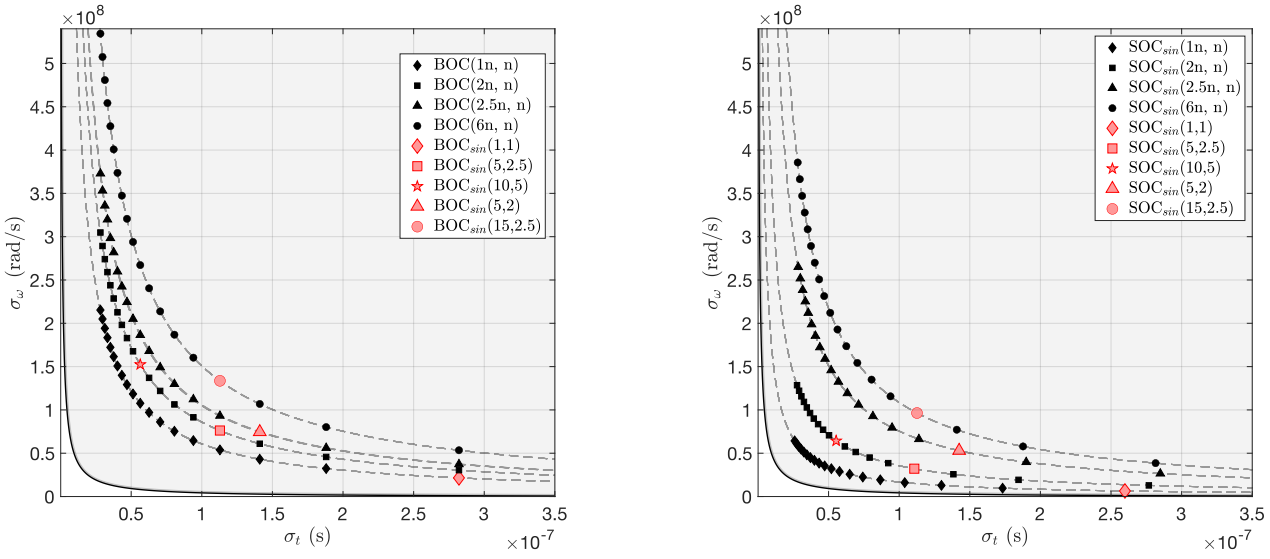

(a) BOC chip shape

(b) SOC chip shape

Figure 3: Time-bandwidth product computed semi-analytically for different carrier offset modulations.

The points highlighted by square, triangular, circular, and rhomboidal markers in Figure 3a and 3b are generated with constant ξ parameter of BOC and SOC modulations. Specifically four values of ξ were selected and are the one shown in table 1. For each values of ξ, modulations of the form BOC($m = \xi n, n$) and SOC($m = \xi n, n$) were generated with n ranging from 1 to 10 in steps of 0.5. Markers such as black rhombus ($\xi = 1$), square ($\xi = 2$), triangle ($\xi = 2.5$) and circle ($\xi = 6$) denote different ξ values. Among all the points, the five corresponding to the reference modulations shown in Table 1 are highlighted.

Eventually, for each point included in the graph, a hyperbola of equation $\sigma_{t_i} \times \sigma_{\omega_i} = TBP_i$ is drawn, where i identifies the i-th tested chip shape and TBP_i denotes its corresponding time-bandwidth product.

Table 2 shows the values of σ_t, σ_ω, the time-bandwidth products, and the Loss in dB (Λ_{dB}). The Loss is defined as the ratio between the time-bandwidth product of the selected modulation (TBP_i) and that of the Gaussian pulse used as a benchmark (TBP_G), calculated as $\Lambda_{\text{dB}} = 10\ \log_{10}\left(\frac{TBP_i}{TBP_G}\right)$.

From Figure 3, it is evident that points associated with the BOC($\xi_i n,\ n$) and SOC($\xi_i n,\ n$) modulations, (i.e., with the same ξ parameter) tend to align on the same hyperbola as n varies. This indicates consistent behavior of the time-bandwidth product with varying chip rates.

Moreover, an increase of the parameter $m = \xi n$, results in an improvement of temporal localization which in graphical terms translates into a point moving to the left on the corresponding hyperbola.

Table 2 and Figure 3 also suggest that time-bandwidth product increases with an increasing ξ. Consequently, points a on the hyperbola associated with the modulations having a higher ξ will always exhibit worse performance as shown by the loss values Λ (dB) reported in Table 2. Λ (dB) for the selected modulations. It is important to note that the loss values shown in the table do not apply only to specific modulations, but represent the entire class of modulations with the same ξ parameter. This highlights how modulations within the same family and with the same value of ξ, for a given sampling frequency F_s, exhibit a constant loss with respect to the benchmark set by the Gaussian pulse, regardless of the value of the chip rate.

2. Analysis of the Cramér-Rao Lower Bound

In the analysis of the CRLB, Figures 4 display the values obtained by applying the square root to the CRLB formulas from (12) and (14). Tables 4 and 3 present the C/N_0 values for both σ_Θ and σ_Ω.

The results reveals a clear decreasing trend in CRLB values as the C/N_0 increases, consistent with the (12) and (14) formulas.

As observed in Figure 3,since we are focusing on a time extension limited to T_c, the spread in the time domain is relatively small. This directly influences the σ_Ω values reported in Table 3.

Table 2: Parameters associated with the selected modulations.

Modulation	σ_t	σ_ω	TBP	Λ_{dB}
Gaussian	-	-	0.5	-
$\text{BOC}_{\text{sin}}(1,1)$	2.821e-07	2.1531e+07	6.073	10.844
$\text{BOC}_{\text{sin}}(5,2.5)$	1.1284e-07	7.6206e+07	8.599	12.354
$\text{BOC}_{\text{sin}}(10,5)$	5.6419e-08	1.5241e+08	8.599	12.354
$\text{BOC}_{\text{sin}}(5,2)$	1.4105e-07	7.4578e+07	10.519	13.230
$\text{BOC}_{\text{sin}}(15,2.5)$	1.1284e-07	1.3361e+08	15.076	14.793
$\text{SOC}_{\text{sin}}(1,1)$	2.5986e-07	6.4277e+06	1.670	5.237
$\text{SOC}_{\text{sin}}(5,2.5)$	1.1071e-07	3.2138e+07	3.558	8.522
$\text{SOC}_{\text{sin}}(10,5)$	5.5354e-08	6.4277e+07	3.558	8.522
$\text{SOC}_{\text{sin}}(5,2)$	1.4245e-07	5.2998e+07	7.549	11.789
$\text{SOC}_{\text{C}}(15,2.5)$	1.1262e-07	9.6415e+07	10.858	13.367

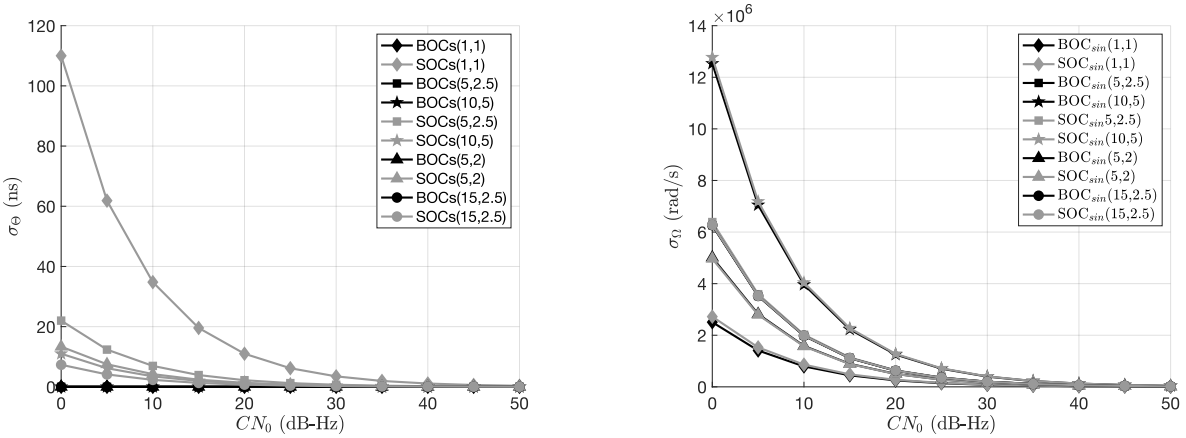

(a) Time delay CRLB

(b) Frequency offset CRLB

Figure 4: CRLBs for time delay and frequency offset estimation of the selected offset carrier modulations.

The relationship between localization in the time and frequency domains and the variances in the estimation is clearly evident when observing the σ_Θ values. Comparing SOC modulations with BOC modulations, we observe that σ_Θ is smaller for SOC than for its BOC counterparts.

Figure 3 illustrates that SOC modulations not only have smaller time-bandwidth product compared to BOC but are also more localized in frequency. This translates into a lower variance in the time delay estimation for BOC compared to SOC.

V. CONCLUSIONS

In this paper, we developed a semi-analytical methodology to evaluate chip shaping performance based on the time-frequency localization principle. We analyzed several state-of-the-art modulations in GNSS by comparing them to reference Gaussian pulses, that theoretically achieve the best performance according to the uncertainty principle. The results suggest that SOC modulations achieve better performance in terms of the time-bandwidth product, but in terms of delay estimation, for the same ξ parameter, they perform worse than the corresponding BOC modulations. Moreover, the proposed semi-analytical analysis demonstrates that the relative performance of various offset carrier modulation schemes remains invariant with respect to the chip duration, thus to the code chip rate. This implies that the fundamental performance bounds, established through comparison against the Gaussian pulse, are consistent and reliable regardless of the chosen chip rate. Consequently, our findings suggest

Table 3: Time delay CRLB (σ_Θ) values for 6 values of C/N_0 (dB-Hz)

	Time delay CRLB (ns)					
C/N_0 (dB-Hz)	**5**	**10**	**20**	**30**	**40**	**50**
$\text{BOC}_{\text{sin}}(1,1)$	18.468	10.386	3.2842	1.0386	0.3284	0.1038
$\text{SOC}_{\text{sin}}(1,1)$	61.863	34.788	11.001	3.4788	1.1001	0.3478
$\text{BOC}_{\text{sin}}(5,2.5)$	5.2179	2.9342	0.9278	0.2934	0.0927	0.0293
$\text{SOC}_{\text{sin}}(5,2.5)$	12.373	6.9576	2.2002	0.6957	0.2200	0.0695
$\text{BOC}_{\text{C}}(10,5)$	2.6089	1.4671	0.4639	0.1467	0.0463	0.0146
$\text{SOC}_{\text{C}}(10,5)$	6.1863	3.4788	1.1001	0.3478	0.1100	0.0348
$\text{BOC}_{\text{C}}(5,2)$	5.3318	2.9983	0.9481	0.2998	0.0948	0.0299
$\text{SOC}_{\text{C}}(5,2)$	7.5029	4.2192	1.3342	0.4219	0.1334	0.0422
$\text{BOC}_{\text{C}}(15,2.5)$	2.9762	1.6736	0.5292	0.1674	0.0529	0.0167
$\text{SOC}_{\text{C}}(15,2.5)$	4.1242	2.319	0.7334	0.2319	0.0733	0.0232

Table 4: Frequency offset CRLB(σ_Ω) values for 6 values of C/N_0 (dB-Hz)

	Frequency offset CRLB (rad/s)					
C/N_0 (dB-Hz)	**5**	**10**	**20**	**30**	**40**	**50**
$\text{BOC}_{\text{sin}}(1,1)$	1.4096e+06	7.9266e+05	2.5066e+05	7.9266e+04	2.5066e+04	7.9266e+03
$\text{SOC}_{\text{sin}}(1,1)$	1.5302e+06	8.6050e+05	2.7211e+05	8.6050e+04	2.7211e+04	8.6050e+03
$\text{BOC}_{\text{sin}}(5,2.5)$	3.5239e+06	1.9817e+06	6.2665e+05	1.9817e+05	6.2665e+04	1.9817e+04
$\text{SOC}_{\text{sin}}(5,2.5)$	3.5918e+06	2.0198e+06	6.3872e+05	2.0198e+05	6.3872e+04	2.0198e+04
$\text{BOC}_{\text{C}}(10,5)$	7.0479e+06	3.9633e+06	1.2533e+06	3.9633e+05	1.2533e+05	3.9633e+04
$\text{SOC}_{\text{C}}(10,5)$	7.1835e+06	4.0396e+06	1.2774e+06	4.0396e+05	1.2774e+05	4.0396e+04
$\text{BOC}_{\text{C}}(5,2)$	2.8191e+06	1.5853e+06	5.0132e+05	1.5853e+05	5.0132e+04	1.5853e+04
$\text{SOC}_{\text{C}}(5,2)$	2.7914e+06	1.5697e+06	4.9638e+05	1.5697e+05	4.9638e+04	1.5697e+04
$\text{BOC}_{\text{C}}(15,2.5)$	3.5239e+06	1.9817e+06	6.2665e+05	1.9817e+05	6.2665e+04	1.9817e+04
$\text{SOC}_{\text{C}}(15,2.5)$	3.5307e+06	1.9855e+06	6.2786e+05	1.9855e+05	6.2786e+04	1.9855e+04

that the evaluation of modulation schemes can be conducted without the necessity of considering the specific chip rate, thereby simplifying the performance analysis and ensuring its applicability across different configurations. This insight has significant implications for the design future navigation signals, as it allows for a more streamlined assessment of modulation techniques, ensuring robust and predictable performance metrics across varying operational parameters.

VI. APPENDIX

1. Appendix A: Variance formulations

This appendix aims to show equality between (3) and (7) and (4) and (8), respectively. By expanding (3) we have:

$$\begin{aligned}
\sigma_t^2 &= \int_{-\infty}^{+\infty} (t - t_0)^2 \, p_t(t) \, dt \\
&= \int_{-\infty}^{+\infty} (t^2 - 2\, t\, t_0^2 + t_0^2) \, p_t(t) \, dt \\
&= \int_{-\infty}^{+\infty} t^2 \, p_t(t) \, dt - 2t_0 \int_{-\infty}^{+\infty} t \, p_t(t) \, dt + t_0^2 \int_{-\infty}^{+\infty} p_t(t) \, dt \\
&= \int_{-\infty}^{+\infty} t^2 \, p_t(t) \, dt - 2t_0^2 + t_0^2 \\
&= \int_{-\infty}^{+\infty} t^2 \, p_t(t) \, dt - t_0^2 \\
&= \int_{-\infty}^{+\infty} t^2 \, p_t(t) \, dt - \left[\int_{-\infty}^{+\infty} t \, p_t(t) dt \right]^2
\end{aligned}$$

By following similar steps starting from (4) it is possible to derive (8).

2. Appendix B: Invariance of the Time-Bandwidth Product to Time and frequency Shifts

This appendix aims to show the invariance of the product band time to time and frequency shift. Before seeing how the square of RMS duration changes, let us focus on how the mean varies. Let the signal $s(t)$ with mean t_0 be shifted by a quantity τ. We denote by t_0' the average of the shifted signal, which will have the form:

$$t_0' = \frac{\int_{-\infty}^{+\infty} t \, |s(t-\tau)|^2 dt}{E_t} \tag{22}$$

applying a change of variable and defining $\psi = t - \tau$, the integral in (22) can be rewritten as:

$$\begin{aligned}
t_0' &= \frac{\int_{-\infty}^{+\infty} (\psi + \tau) \, |s(\psi)|^2 \, d\psi}{E_t} \\
&= \frac{\int_{-\infty}^{+\infty} \psi \, |s(\psi)|^2 \, d\psi}{E_t} + \frac{\int_{-\infty}^{+\infty} \tau \, |s(\psi)|^2 \, d\psi}{E_t} \\
&= t_0 + \tau \frac{\int_{-\infty}^{+\infty} |s(\psi)|^2 \, d\psi}{E_t} \\
&= t_0 + \tau
\end{aligned} \tag{23}$$

From the result in (23) it is possible to rewrite the expression for the RMS duration as:

$$
\begin{aligned}
\sigma_{\tau}^{'2} &= \frac{1}{E_t} \int_{-\infty}^{+\infty} (t - t_0 - \tau)^2 \, |s(t-\tau)|^2 \, dt \\
&= \frac{1}{E_t} \int_{-\infty}^{+\infty} (\psi - t_0)^2 \, |s(\psi)|^2 \, dt \\
&= \sigma_{\tau}^2
\end{aligned}
\tag{24}
$$

Furthermore, given that a time shift reflects in the frequency domain as a multiplication by a complex exponential, specifically $e^{j\omega\tau}$, it is evident that the magnitude of the Fourier transform of the signal is unaffected, but only its phase changes. This phase change does not impact our calculation. In other words, it can be concluded that the time-bandwidth product is invariant with respect to a time shift.

Regarding the signal shift in frequency by an ω_1 frequency, i.e., $S(\omega - \omega_1)$, one can proceed with a similar reasoning as that done for the time domain and conclude that it does not affect the time-bandwidth product.

ACKNOWLEDGEMENTS

A. Minetto acknowledges funding from the research contract no. 32-G-13427-5 DM 1062/2021 funded within the Programma Operativo Nazionale (PON) Ricerca ed Innovazione of the Italian Ministry of University and Research (MUR).

This paper is part of the project NODES which has received funding from the MUR – M4C2 1.5 of PNRR funded by the European Union - NextGenerationEU (Grant agreement no. ECS00000036)

REFERENCES

Angelo, J. (2010). Measuring GNSS signal strength. `https://insidegnss.com/wp-content/uploads/2018/01/novdec10-Solutions.pdf`.

Ávila Rodríguez, J. Á. (2008). *On generalized signal waveforms for satellite navigation*. PhD thesis, München, Univ. der Bundeswehr, Diss., 2008.

Boggess, A. and Narcowich, F. J. (2015). *A first course in wavelets with Fourier analysis*. John Wiley & Sons.

Gabor, D. (1946). Theory of communication. *Journal of Institution of Electrical Engineers*, 93:429–457.

Haddad, R. A., Akansu, A. N., and Benyassine, A. (1993). Time-frequency localization in transforms, subbands, and wavelets: a critical review. *Optical Engineering*, 32(7):1411–1429.

Hegarty, C. J. (2012). Gnss signals — an overview. In *2012 IEEE International Frequency Control Symposium Proceedings*, pages 1–7.

Heissenberg, W. (1930). The physical principles of quantum theory.

Kennard, E. H. (1927). Zur quantenmechanik einfacher bewegungstypen. *Zeitschrift für Physik*, 44(4):326–352.

Levanon, N. (1988). *Radar principles*. New York.

Luise, M. and Vitetta, G. (2009). *Teoria dei segnali*. Collana di istruzione scientifica. McGraw-Hill Companies.

McDonough, R. and Whalen, A. (1995). *Detection of Signals in Noise*, pages 383–445. Elsevier Inc., Amsterdam.

Papoulis, A. (1977). *Signal Analysis*. Electrical & electronic engineering series. McGraw-Hill.

Pratap, M. and Per, E. (2010). *Global Positioning System: Signals, Measurements, and Performance*. Ganga-Jamuna Press.

Robertson, H. P. (1929). The uncertainty principle. *Physical Review*, 34(1):163.

Ross, S. (2010). *A First Course in Probability*. Pearson Prentice Hall.

Yao, Z. and Lu, M. (2021). *Next-Generation GNSS Signal Design*. Springer.

Zhang, X., Yao, Z., and Lu, M. (2011a). Optimizing the Gabor bandwidth of satellite navigation signals by MCS signal expression. *Science China Physics, Mechanics and Astronomy*, 54:1077–1082.

Zhang, X., Yao, Z., Zhang, X., and Lu, M. (2011b). A method to optimize the spreading code chip waveform in sense of Gabor bandwidth. In *Proceedings of the 24th international technical meeting of the satellite division of the institute of navigation (ION GNSS 2011)*, pages 1299–1304.

Zocca, S., Guo, Y., Minetto, A., and Dovis, F. (2022). Improved weighting in particle filters applied to precise state estimation in GNSS. *Frontiers in Robotics and AI*, 9:950427.